19th Australasian Fluid Mechanics Conference
Melbourne, Australia
8-11 December 2014

Drag Reduction of a Turbulent Boundary Layer Using Plasma Actuators

Y.P. Li [1], C.W. Wong[1], Y.Z. Li[1], B.F. Zhang[2] and Y. Zhou[1]

[1]Institute for Turbulence-Noise-Vibration Interactions and Control
Shenzhen Graduate School, Harbin Institute of Technology, Shenzhen, 518055, P.R. China
[2]Department of Mechanical Engineering, The Hong Kong Polytechnic University, Hong Kong

Abstract

This work aims to manipulate using plasma actuators a fully developed turbulent boundary layer over a flat plate, with a view to reduce the friction drag. Four different plasma actuator configurations were designed to generate streamwise vortices. While the time-resolved PIV was used to capture the development and interaction of streamwise vortices in a plane normal to the mean flow, a surface balance technique was deployed to measure the skin-friction drag. A new calibration method is proposed for this technique to resolve accurately the friction drag change. It has been found that the plasma-actuator-generated vortices and their interactions with the boundary layer may lead to a drag reduction up to 50%. The control efficiency is also estimated.

Introduction

The key contributor to global warming is a direct function of fuel consumption by transportations; apparently fuel saving by viscous drag reduction could minimize such problem, and yet, effective drag reduction technique could cut down the fuel cost, particularly for airlines. Thus, viscous drag reduction of turbulent boundary layer has received widespread attention.

Sweep and ejection events are closely associated with the bursting process occurring at 15 wall units above the wall [1], thus manipulating the near wall region could directly affect the process of ejection and sweep. Based on numerical simulation, Choi et al. (1994) [2] applied blowing and suction over a surface in a turbulent channel flow, and achieved approximately 20-30% skin friction drag reduction. Berger et al. (2000) [3] applied oscillating Lorentz forces in the near-wall region of a turbulent channel flow, and the skin-friction drag was reduced by about 40%. Choi & Clayton (2001) [4] investigated the turbulent boundary layer over a spanwise oscillating wall, within which the net spanwise vorticity was generated by the periodic Stokes layer. The skin-friction coefficient was reduced by 45%. By applying streamwise vortices in the turbulent channel flow, Schoppa & Hussain (1998) [5] and Iuso et al. [6] achieved the skin-friction drag reduction of about 20-30%. Likewise, Di Cicca et al. (2002) [7] investigated the large-scale longitudinal vortices embedded in the flat-plate turbulent boundary layer, and the skin-friction was also reduced. Recently, Choi et al. (2011) [8] applied spanwise oscillation and spanwise travelling wave with DBD plasma actuators for skin-friction reduction in turbulent boundary layer. For the spanwise oscillation study, the spanwise oscillation took place within the viscous sublayer and in the buffer layer, disrupting the sweep and ejection events. For the spanwise travelling wave study, starting vortices were created in sequence by plasma actuators, and these vortices reduced the mean velocity in the buffer and lower log region. Both plasma arrangements resulted skin-friction reduction up to 45%.

In this paper, four DBD plasma actuators were designed, with a view to reduce the friction drag in a turbulent boundary layer based on plasma-actuator-generated streamwise vortices. A surface balance, built in house, was used to measure the averaged skin-friction drag immediately behind the plasma actuators. A new calibration method was proposed for this technique to resolve accurately the friction drag change. By adjusting the input voltage of the plasma actuators, the development and interactions between the induced vortices altered, thus reducing the skin friction drag. Finally, the control efficiency was estimated based on the measurement of total power consumption for each plasma actuator.

Experimental Details

Experiments were performed in the closed-loop wind tunnel, with a working section of $L \times W \times H = 5.5 \times 0.8 \times 1.0$ m, at the Institute for Turbulence-Noise-Vibration Interactions and Control, Shenzhen Graduate School, Harbin Institute of Technology. A flat plate made of PMMA with $L \times W \times H = 4.8 \times 0.78 \times 0.015$ m was installed horizontally (unless otherwise noted) in the test section. The leading edge of the flat-plate was designed with an elliptic geometry with an ellipticity of 1:4 to avoid flow separation, and an adjustable end plate ($L = 0.2$ m) was used to ensure zero pressure gradient. Two rows of screws were installed at $x = 100$ mm downstream of the leading edge of the flat-plate to generate fully developed turbulent boundary-layer at the measurement station ($x = 3.2$ m) in the freestream velocity U_∞ of 2.4 m/s. The boundary layer thickness δ was 85 mm at the measurement station, while the Reynolds number based on momentum thickness $Re_\theta = 1100$, and the wall unit $l^* = 150$ μm.

The DBD plasma actuators used in the experiments composed of two copper electrodes, each 23 μm thick, separated by a dielectric panel, which consisted of three layers of two dielectric materials: 73 μm thick Mylar sheet was placed between two Kapton sheets 55 μm thick, giving an overall thickness of about 230 μm ($\approx 1.5l^*$), and hence the influence due to the protuberance of the actuator sheet to the flow was negligible. Plasma was formed by applying steady sinusoidal AC waveforms to the upper electrodes with $E = 3.00$ - 7.84 $kV_{p\text{-}p}$ at frequencies $f = 11$ kHz, while the lower electrodes were connected to ground. Four different plasma configurations, i.e., A, B, C and D, were investigated, and schematics of the four plasma configurations are given in figure 1. A is a totally colliding counter-rotating vortex generator, and the plasma-induced streamwise vortices of an actuator collide with those generated by the opposite actuator along the entire length of the actuator. B is a midway-colliding counter-rotating vortex generator, and the plasma-induced streamwise vortices of an actuator collide with those by the opposite actuator at a location approximately half of the actuator length. C is a non-colliding co-rotating vortices generator and vortices generated by one actuator do not appear interfering with those by the neighboring actuator. D is a sawtooth plasma actuator, comprised of two sawtooth electrodes arranged such that the opposite sawtooths point at each other. The actuator could induce streamwise flow and counter-rotating vortex pairs at the tip and adjacent to the tip, respectively.

Further details of plasma configuration D could be found in Wong et al. (2014) [9]. Note that the trailing edges of the upper electrodes of all actuators were placed at 15 mm upstream of the measurement station.

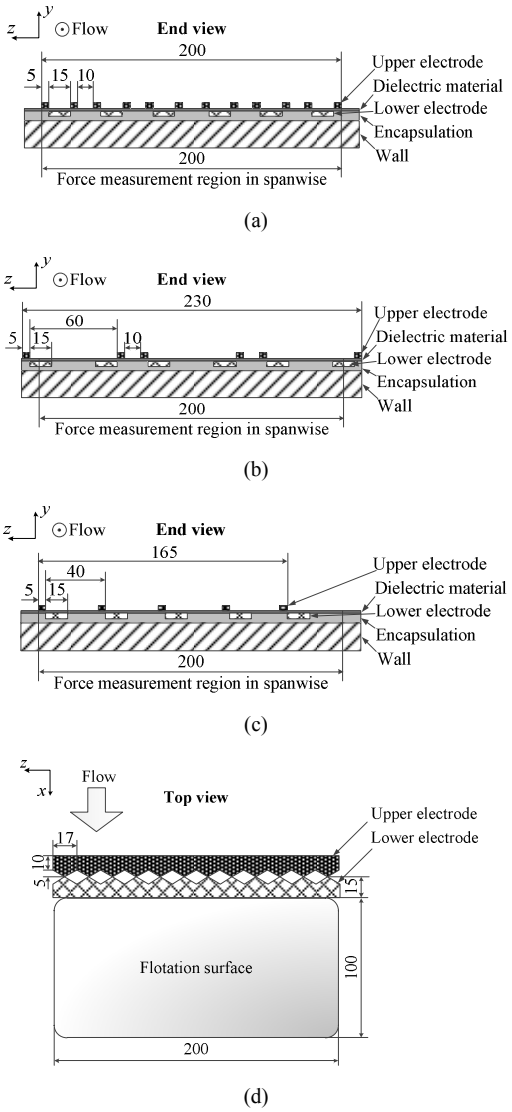

Figure 1. Four plasma configurations: (A); (B); (C); (D).

The flow field behind a single DBD plasma actuator oriented longitudinally in a laminar boundary layer was investigated by Jukes & Choi (2013) [10], however, the induced flow field could be significantly different compared to that generated in the turbulent boundary layer, and so, it was necessary to study one single DBD plasma actuator in turbulent boundary layer. The flow field generated by configuration B was more complex than that of A. Therefore, the induced flow field by configuration B was studied using 2-D particle image velocimetry. A pair of actuators of configuration B was attached at x = 2985 mm (figure 2). In order to facilitate the PIV measurement, the flat-plate was installed vertically inside the test section. The camera and the laser were mounted on the side and on the top of the test section, respectively, and captured the y-z plane via a 0.94 δ×1.41 δ (8×12 mm) high-quality mirror located at x = 4998 mm and mounted at 45° to the x-z plane. A total of five y-z planes were studied. The trigger rate of the PIV was 300 Hz under double frame mode, and 300 images were acquired for each plane studied.

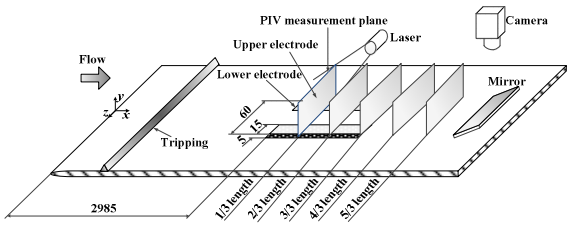

Figure 2. Schematic of experimental setup for PIV measurement.

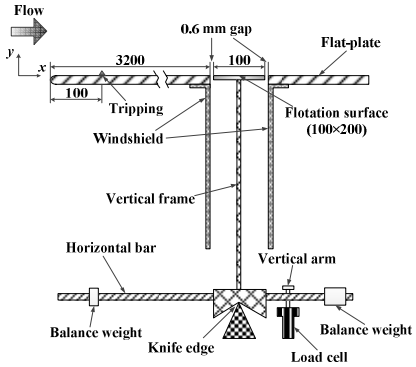

Figure 3. Schematic of experimental setup for skin friction measurement using surface balance.

A Surface balance was used to measure the averaged skin-friction drag over an area covering 0.02 m^2 at x = 3200 mm (figure 3). The gap between the flotation surface and the flat-plate was 0.6 mm. The skin-friction drag sensed by the flotation surface was based on the lever principle, as such, force transmitted through the vertical frame and onto the sharp knife edge, where the amplified force was measured by the load cell (Honeywell Model 34, range ±1kg). The amplified output signal with an accuracy of ±0.01%, and was acquired by the NI data acquisition card, with the sampling frequency and the sample time at 2000 Hz and 180 s, respectively. In the current study, the measured force over the flotation surface was significantly less than 1 g. In order to resolve accurately the small skin-friction drag (order of 10^{-4} N), a calibration method was proposed for the surface balance. Firstly, the velocity profiles at the measurement station were measured at U_∞ = 2.4 m/s and 5 m/s. The velocity profiles were then fitted into the logarithmic portion of the profile to the 'universal' velocity profile. We chose the Clauser's equation (1956) [11],

$$\overline{U}^+ = 2.44 \ln y^+ + 4.9 \tag{1}$$

where

$$\overline{U}^+ = \overline{U} / u_\tau \tag{2}$$

$$y^+ = y u_\tau / \nu \tag{3}$$

and u_τ is the shear velocity, ν is the kinematic viscosity of air. Then we can determine

$$\frac{\overline{U}}{u_\tau} = 2.44 \ln\left(\frac{u_\tau}{\overline{U}}\right) + 2.44 \ln\left(\frac{\overline{U} y}{\nu}\right) + 4.9 \tag{4}$$

Based on equation (4), we can establish the local value of u_τ. The values of u_τ were plotted versus y, and yielded a constant value in the log region, from which the shear velocity u_τ can be determined [12]. Then we calibrated the surface balance system through the skin-friction drag F estimated by the shear velocity u_τ, based on

$$F = \rho u_\tau^2 A \tag{5}$$

where ρ is the air density, A is the area of flotation surface. The calibration curve is linear as shown in figure 4.

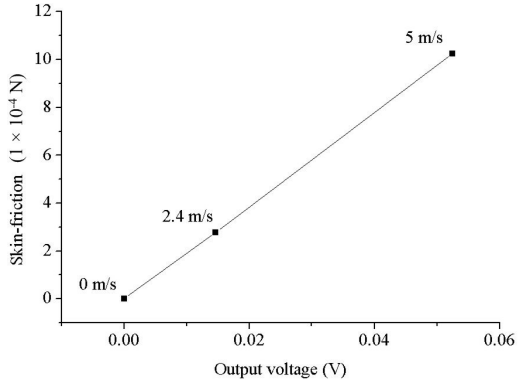

Figure 4. The calibration curve of surface balance system.

The ratio of skin-friction to output voltage of the system is 0.01952 N/V, and the accuracy of the system is as high as $\pm 1.5\times10^{-5}$ N (about ±2% of the skin-friction drag on the flotation surface under U_∞ = 2.4 m/s without control).

In order to estimate the control efficiency, the total power consumption of each plasma actuator configuration was obtained through the measurement of the applied voltage and current using high voltage probe (Trek, P6015A) and current probe (Trek, P6021), respectively. The current was deduced from the voltage across a non-inductive resistor (100 Ω) connected in series between the lower electrode and the earth. Both waveforms were recorded using a digital oscilloscope. The total electrical power consumption of each actuator used in the experiment was computed with the following equation [13];

$$P = \frac{1}{T}\int_{t=0}^{T} v(t)\times i(t)dt \tag{6}$$

Where, $v(t)$ and $i(t)$ are time dependent voltage and current respectively, and T is the waveform period. Note that 33 cycles were recorded with a time resolution equal to 2 ns.

Results and Discussions

PIV Results

Firstly, let us consider the x-y planes (figure 5a) captured with the plasma configuration B. For the single plasma actuator, the vortex core rose up as it moved downstream. The vortex core trajectory follows the power law $y_c \sim x_c^{2/3}$ (y_c is the height of vortex core; x_c is the distance from the leading edge of upper electrode to the vortex core in streamwise direction), and is consistent with Jukes & Choi (2013) [10]). Note that we estimated $y_c \approx 0.012\delta$ at $x_c = 0$, which is somewhat different from Jukes & Choi (2013) [10]. At the same x_c, y_c increases with increasing voltage. For a pair of plasma actuators, the vortex strength was weak at E = 4.5 kV$_{p\text{-}p}$, and therefore, the vortex pair did not collide at all. On the other hand, the vortex core rose up rapidly due to the extrusion when the two vortices came close together or collided. The slope of vortex trajectory increases at x_c = 3/3 and 2/3 for E = 6.0 kV$_{p\text{-}p}$ and 7.5 kV$_{p\text{-}p}$, respectively. Based on the PIV data (not shown), the two vortices stretched in y-direction and compressed in z-direction, and formed elliptical geometry after collision. This eventually promoted the vortex cores lifting up from the surface. Note that the vortex core rose up by about 0.057δ and 0.09δ after collision at E = 6.0 kV$_{p\text{-}p}$ and 7.5 kV$_{p\text{-}p}$, respectively.

In plane x-z (Figure 5b) and for the pair of plasma actuators, the separation between two vortex cores is the smallest at x_c = 2/3 at E = 7.5 kV$_{p\text{-}p}$, thus indicating where the two vortices collided. When two vortices collided, a strong up-wash region was formed and the maximum vorticity shrank from 420 s^{-1} (at x_c = 1/3) to 220 s^{-1} (x_c = 2/3). On the other hand, at E = 6.0 kV$_{p\text{-}p}$ the vortex cores collision leads to the reduction of approaching velocity of the two vortex cores, and the maximum vorticity shrank from 160 s^{-1} (at x_c = 2/3) to 100 s^{-1} (x_c = 3/3).

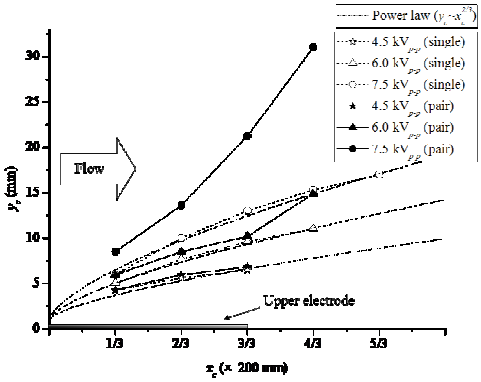

(a)

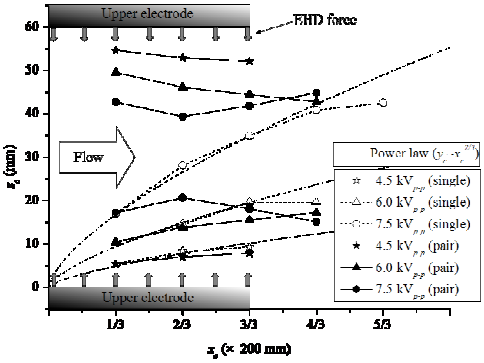

(b)

Figure 5. Vortex core trajectories in (a) x-y plane and (b) x-z plane for plasma configuration B.

Drag Reduction Results

Figure 6 shows the dependence of drag change $\Delta c_f = (F_1\text{-}F_2)/F_2$ on voltage for different plasma configurations, where F_1 and F_2 are the skin-friction drags with and without plasma operated, respectively. Note that due to the difference in total "effective" length of each plasma configuration, the comparison displayed in figure 6 is based on different power consumption. For configurations A, B and C, Δc_f increases rapidly with increasing voltage, particularly at $E \leq$ 4.25 kV$_{p\text{-}p}$. The Δc_f of B is always slightly larger than that of A or C. The induced vortex pair by A formed an upwash region upon collision, which is somewhat similar to a vertical jet, whilst several rows of streamwise vortices, without collision, were induced by B and C, thus reducing the skin-friction drag. The slope of the curves increases suddenly at E = 4.25 kV$_{p\text{-}p}$ for A, B and C, indicating the occurrence of flow separation and reversal, which leads to Δc_f shooting over one. In contrast, the flow separation did not occur for D, whose Δc_f is significantly lower than others though.

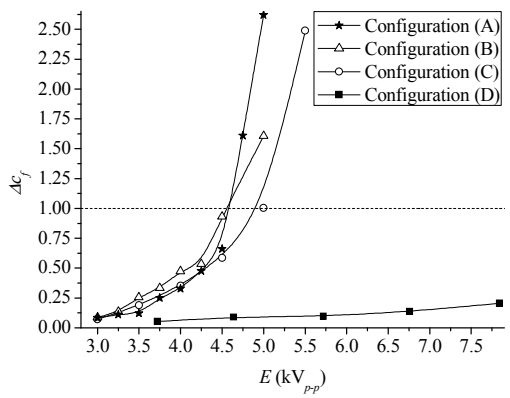

Figure 6. Dependence of drag reduction Δc_f on voltage E for different plasma configurations.

Control Efficiency

In order to examine the control efficiency, $\Delta c_f/P$ was examined for each configuration (figure 7). Configuration A shows the lowest control efficiency of all, whereas B and C are virtually the same. In general, the control efficiency increases initially for higher voltage. But beyond a certain level of voltage, the control efficiency drops, probably because higher voltage produces flow separation in cases of B and C or the streamwise flow induced at the tip of the sawtooth electrode introduces significant additional drag in case of configuration D. The data at $E > 4.5$ kV$_{p\text{-}p}$ has been removed for A, B and C in view of the occurrence of flow separation and reversal.

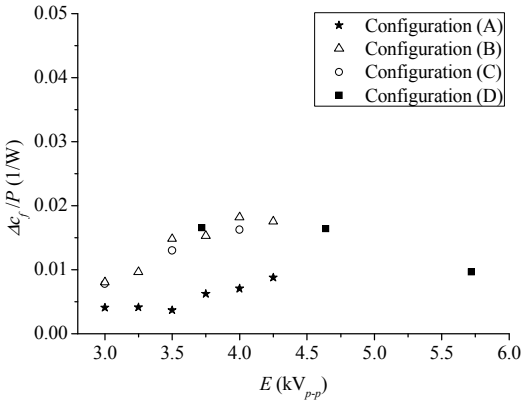

Figure 7. Dependence of the control efficiency $\Delta c_f/P$ on voltage E.

Conclusions

Experimental investigation was performed to manipulate a fully developed flat-plate turbulent boundary-layer using four different plasma actuator configurations. Following conclusions can be drawn:

(1) Of the plasma actuators, the configuration B was able to allow the vortex pair to collide halfway along the electrode length, thus altering their trajectory and formed a wide up-wash region in the middle.

(2) A calibration method was proposed for the surface balance, allowing the accurate resolution of the skin-friction drag up to $\pm 1.5\times10^{-5}$ N.

(3) The plasma configurations A, B, and C resulted in significant drag reduction at $E \leq 4.25$ kV$_{p\text{-}p}$, achieving a maximum drag reduction of about 50%, whilst the configuration D led to a maximum drag reduction of about 20%.

(4) The control efficiency $\Delta c_f/P$ of all four actuator configurations was examined. The control efficiency of configuration A is lowest of the four. The control efficiency of configurations B and C are virtually the same. The control efficiency of configuration D is approximately equal to that of B at $E = 3.75$ kV$_{p\text{-}p}$, but reduced at high voltage due to the shear stress gain caused by the streamwise wall jet at the sawtooths.

Acknowledgments

CW WONG wishes to acknowledge support given to him from Research Grants Council of Shenzhen Government through Grants JC201105160543A, JCYJ20120613153244545 and JCYJ20130402100505796.

References

[1] Wallace J. M., Eckelmann H. & Brodkey R. S., The wall region in turbulent shear flow. *J. Fluid Mech.* **54**: 39-48, 1972.

[2] Choi, H., Moin, P. & Kim, J., Active turbulence control for drag reduction in wall-bounded flows. *J. Fluid Mech*. **262**, 75-110, 1994.

[3] Berger T. W., Kim J., Lee C. & Lim J., Turbulent boundary layer control utilizing the Lorentz force. *Phys. Fluids* **12**, 631-649, 2000.

[4] Choi, K.-S. & Clayton, B. R., The mechanism of turbulent drag reduction with wall oscillation. *International Journal of Heat and Fluid Flow* **22**(1), 1-9, 2001.

[5] Schoppa, W. & Hussain, F., A large-scale control strategy for drag reduction in turbulent boundary layers, *Phys. Fluids* **10**(5), 1049-1051, 1998.

[6] Iuso, G., Onorato, M., Spazzini, P.G. & Di Cicca, G.M., Wall turbulence manipulation by large-scale streamwise vortices, *J. Fluid Mech.* **473**, 23-58, 2002.

[7] Di Cicca, G.M., Iuso G., Spazzini, P.G. & Onorato, M., PIV study of the influence of large-scale streamwise vortices on a turbulent boundary layer, *Exp. Fluids* **33**(5), 663-669, 2002.

[8] Choi, K.-S., Jukes, T. & Whalley, R., Turbulent boundary-layer control with plasma actuators, *Philosophical Transactions of The Royal Society A: Mathematical Physical and Engineering Sciences* **369**(1940), 1443-1458, 2011.

[9] Wong, C.W., Wang, L.J., Wu, Z., Li, C.H., Alam, M.M., Zhou, Y., Control of separated flow on a NACA 0015 airfoil using three-dimensional plasma actuator, *7th AIAA Flow Control Conference* (2014-2665), 2014.

[10] Jukes, T.N. & Choi, K.-S., On the formation of streamwise vortices by plasma vortex generators, *J. Fluid Mech.* **733**, 370-393, 2013.

[11] Clauser, F.H., Advances in Applied Mechanics, New York: Academic Press 4, 1956.

[12] Kline, S.J., Reynolds, W.C., Schraub, F.A. & Runstadler P.W., The structure of turbulent boundary layers, *J. Fluid Mech.* **30**, 741-773, 1967.

[13] Jolibois, J. & Moreau, E., Enhancement of the electromechanical performances of a single dielectric barrier discharge actuator, *IEEE Transactions on Dielectrics and Electrical Insulation* **16**(3), 758-767, 2009.